TECHNISCHE UNIVERSITÄT
KAISERSLAUTERN

SCHRIFTEN ZUR

FUNKTIONALANALYSIS UND GEOMATHEMATIK

M. Gutting, D. Michel (eds.)

Contributions of the Geomathematics Group, TU Kaiserslautern, to the 2nd International GOCE User Workshop 2004 at ESA-ESRIN Frascati, Italy

Bericht 10 – April 2004

FACHBEREICH MATHEMATIK

Contributions of the Geomathematics Group, TU Kaiserslautern, to the 2nd International GOCE User Workshop 2004 at ESA-ESRIN Frascati, Italy

A: Multiscale Modeling of Ocean Circulation

B: Multiscale Modeling from EIGEN-1S, EIGEN-2, EIGEN-GRACE01S, GGM01, UCPH2002_0.5, EGM96

by

A: W. Freeden, D. Michel, V. Michel

B: M. J. Fengler, W. Freeden, M. Gutting

TU Kaiserslautern
Geomathematics Group
P.O. Box 3049
67653 Kaiserslautern
Germany

Abstract

The following two papers present recent developments in multiscale ocean circulation modeling and multiscale gravitational field modeling that have been presented at the 2nd International GOCE User Workshop 2004 in Frascati.

AMS classification: 31B05, 42C40, 65T60, 86A05, 86A30

Keywords: constructive approximation, spherical wavelets, multiscale modeling, geostrophic flow, graviational field recovery

Multiscale Modeling of Ocean Circulation

Willi Freeden[(1)] , Dominik Michel[(1⋆)], and Volker Michel[(1)]

(1) Geomathematics Group, University of Kaiserslautern,
P.O.Box 3049, 67653 Kaiserslautern, Germany
(⋆) D. Michel will give the talk at the GOCE User Workshop.

Abstract

In this paper the applicability of multiscale methods to oceanography is demonstrated. More precisely, we use convolutions with certain locally supported kernels to approximate the dynamic topography and the geostrophic flow. As data sets the French CLS01 data are used for the mean sea surface topography and are compared to the EGM96 geoid. Since those two data sets have very different levels of spatial resolutions the necessity of an interpolating or approximating tool is evident. Compared to the standard spherical harmonics approach, the strongly space localizing kernels improve the possibilities of local data analysis here.

Keywords: Dynamic Topography, Geostrophic Flow, Multiscale Modeling, Constructive Approximation, Locally Compact Kernel Functions

1 INTRODUCTION

As a crucial factor for resource mining, industry and recreation, weather and climate, the oceans are of immediate importance. Modeling data sets on the sphere (and in a first approximation the regions under consideration are part of a spherically shaped Earth), the question arises how to describe scalar (or analogously vectorial) functions on it. Commonly, spherical functions are expanded into a Fourier series of spherical harmonics. But the polynomials, restricted to the sphere, are, though the obvious choice for a suitable ansatz space, globally defined. Actually, oceanic phenomena are regionally dominated, thus continental parts have to be left outside. Further, basis functions with global support tend to spread errors from a certain region around the whole sphere. Thus, a new set of basis functions has to be considered, reflecting more than the common ones the bounded regions we are considering. Further, spherical harmonics give immediate access to the spectral behavior of the signal (since obtaining optimal frequency localization), but have no intrinsic and suitable low-pass filter. Thus, a new method of approximating the signal is necessary, leaving the spectral ansatz. By introducing a multiscale way of approximation we provide special handling of (and a separation between) the long-wavelength and the high-frequency parts.

2 PRELIMINARIES

In the common way we introduce the notation necessary for this paper. As usual, $\mathbb{N}$ and $\mathbb{R}$ denote the set of integers and real numbers. As function spaces the sets of all square-integrable functions over a certain domain are mainly used, i.e. generally the space of all functions $F : D \to \mathbb{R}$ for a compact subset $D \subset \mathbb{R}^n$, fulfilling the property $\int_D |F(x)|^2 dx < \infty$. These spaces, denoted as $\mathcal{L}^2(D)$, are Hilbert spaces, equipped with the scalar product $< \cdot, \cdot >_{\mathcal{L}^2(D)}$. Within the context of this paper, there are two possible domains D.
At first we consider the real interval $[-1, +1]$. The common set of orthogonal basis functions of the space $(\mathcal{L}^2([-1,1]), < \cdot, \cdot >_{\mathcal{L}^2([-1,1])})$ is obviously given by the Legendre polynomials (see e.g. [3]).
The second one is the unit sphere Ω. For the closed and complete set of basis functions for this Hilbert space $(\mathcal{L}^2(\Omega), < \cdot, \cdot >_{\mathcal{L}^2(\Omega)})$ spherical harmonics, homogeneous harmonic polynomials in $\mathbb{R}^3$ restricted to the unit sphere, can be chosen. As known, for each degree n the space of these polynomials has the dimension $2n + 1$, i.e. the basis system carries two indices instead of one.
For both spaces each element F can be expanded in terms of a Fourier series including the basis functions and corresponding coefficients, which are denoted by $F^\wedge(n)$, resp. $F^\wedge(n, k)$.
As a further property, the set of all continuous functions on $[-1, 1]$, resp. Ω, is a dense subset of the space of all square-integrable functions. Generally, $\mathcal{C}^n(D)$ denotes the set of all n-times continuously differentiable real-valued functions on D.
Within spherical notation, differential operators change their appearance. The gradient ∇ separates into a radial part $\xi \frac{\partial}{\partial r}$ and a horizontal part $\frac{1}{r}\nabla^\star_\xi$, where $x = r\xi$, $\xi \in \Omega$, for $x \neq 0$. Moreover, the so-called *surface curl gradient* $L^\star$ is defined as $L^\star_\xi = x \wedge \nabla_x|_{x=r\xi} = \xi \wedge \nabla^\star_\xi$, where $\wedge$ denotes the standard vector cross product in $\mathbb{R}^3$.

3 MULTISCALE APPROXIMATION

Modeling measurements on the sphere implies finding an appropriate function within a certain space that fits properly. This is commonly done by the Hilbert space $\mathcal{L}^2(\Omega)$. Instead of an approximation by a Fourier series we want to introduce here another tool, the multiscale approximation. Although the first part of this section is written for arbitrary (though they have to fulfill certain, here not mentioned conditions) radial basis functions, the second part is concerned with a very simple kernel function, the locally supported Haar function.

3.1 (Spatial) Multiscale Analysis

Definition 1 *Let $\{K_h\}_{h\in(-1,1)} \subset \mathcal{L}^2([-1,1])$ be a family of kernel functions satisfying the condition $\int_{-1}^{1} K_h(t)dt = \frac{1}{2\pi}$ for all $h \in (-1,1)$. Then we may define the convolution with a function $F \in \mathcal{L}^2(\Omega)$ as a (spherical) singular integral in the following way*

$$I_h(F)(\xi) := (K_h \star F)(\xi) := \int_\Omega K_h(\xi \cdot \eta)F(\eta)d\omega(\eta) \quad . \tag{1}$$

For an unknown function $F \in \mathcal{L}^2(\Omega)$ the convolution with a kernel function represents a weighted and smoothed approximation. Under certain conditions, this approximation converges for $h \to 1$ ($h < 1$) to the function itself. Then the following condition is satisfied.

Definition 2 *The singular integral is said to be an approximate identity (in $\mathcal{L}^2(\Omega)$) corresponding to the scaling function $\{K_h\}_{h\in(-1,1)}$, if the following limit relation holds true:*

$$\lim_{\substack{h\to 1\\ h<1}} ||F - I_h(F)||_{\mathcal{L}^2(\Omega)} = 0 \tag{2}$$

for all $F \in \mathcal{L}^2(\Omega)$.

Roughly spoken, the kernel function has to be an approximation of the Dirac functional in $\mathcal{L}^2$, i.e. in the limit we have $\lim_{h\to 1,h<1} K^\wedge(n) = 1$ for all $n \in \mathbb{N}_0$. By choosing the way of convergence for Fourier coefficients of the scaling function the possibilities of this approximation ansatz are wide-spread. For more details on approximate identities and for the spectral approach to multiscale analysis we refer for example to [3, 4].

The approximate identity represents a continuous method to model the function under consideration with a set of basis functions. To obtain a discrete multiscale approximation we force h to have a certain structure. Commonly, this subdivision is dyadic, i.e. $h_J := 1 - 2^{-J}$ for all $J \in \mathbb{N}_0$.
This step-structure we introduced gives the possibility to talk about detail information. In each scale we convolve the function with a spherical cap, smoothing it over a small area. This becomes smaller with increasing J, i.e. the solution becomes more detailed. Since convolutions are linear in both arguments, we can cluster the difference between two scaling functions to a wavelet. By convolving this wavelet with the function we obtain the details its approximation gains from one step to the next.
Though several families of kernel functions are possible for multiscale approximations we want to restrict ourselves here to a certain class. Their fundamental property is stated in the following theorem, which can also be found in [4].

Theorem 3 *Let $\{K_h\}_{h\in(-1,1)}$ be a family of functions in $\mathcal{L}^2([-1,1])$, which satisfy $\int_{-1}^{1} K_h(t)dt = \frac{1}{2\pi}$ for all $h \in (-1,1)$ and which are non-negative. Let $\{I_h\}_{h\in(-1,1)}$ be the corresponding spherical singular integral. Then the following properties are equivalent:*

- *$\{I_h\}_{h\in(-1,1)}$ is an approximate identity,*
- *$\lim_{h\to 1,h<1}(K_h)^\wedge(n) = 1$ for all $n \in \mathbb{N}_0$,*
- *$\{K_h\}_{h\in(-1,1)}$ satisfies the localization property $\lim_{h\to 1,h<1} \int_{-1}^{\delta} K_h(t)dt = 0$ for all $\delta \in (-1,1)$.*

Thus, kernel functions with a support of $[h,1]$, i.e. locally supported kernel functions, are obviously predetermined families for multiscale approximations.

3.2 Locally Supported Kernel Functions

The scaling function under consideration is the simplest locally supported kernel function, the hat function devolved on the sphere.

Definition 4 *The smoothed Haar scaling function (non-band-limited, locally supported kernel function) is defined by*

$$L_h^{(k)}(t) := \begin{cases} 0 & \text{if } t \in [-1, h) \\ \frac{k+1}{2\pi} \frac{(t-h)^k}{(1-h)^{k+1}} & \text{if } t \in [h, 1] \end{cases} \tag{3}$$

with $h \in [-1, 1)$ and $k \in \mathbb{N}_0$ such that $L_h^{(k)} \in \mathcal{C}^{k-1}([-1, 1])$. Here, the upper index indicates neither derivative nor iterated convolution, but just a continuity parameter.
It can be shown, that $|(L_h^{(k)})\hat{}(n)| = \mathcal{O}([n(1-h)]^{-3/2-k})$ for $n \to \infty$, as seen in [4].

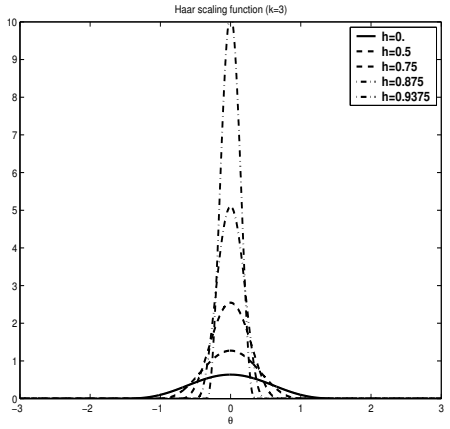

Figure 1: Spatial shape of the Haar kernel over θ, i.e. $t = \cos\theta$

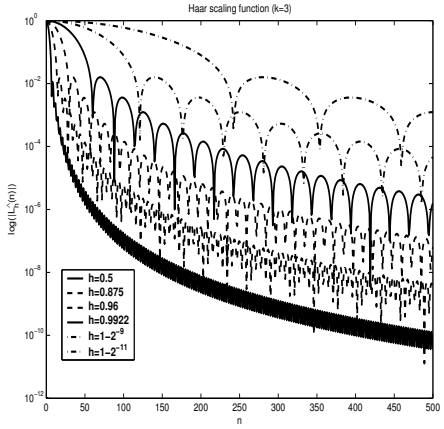

Figure 2: Symbol of the Haar scaling function for scales 0 to 7 (logarithmic view).

For further details on multiscale analysis and locally supported kernel functions, including the more complex function types, we refer exemplarily to [2, 3, 4].

4 MODELING THE DYNAMIC TOPOGRAPHY

As a scalar field on the sphere, the dynamic topography, represented commonly as an expansion in spherical harmonics, is an ideal candidate for illustrating the methods presented above. Basically, it consists of two measurements. On the one hand, on an Earth at rest, the water masses would align along the geoid, the equipotential surface of the Earth's gravity field. Its deviation from the standard reference ellipsoid (the first approximation of the Earth's shape) is called geoid undulation. On the other hand, satellite measurements provide altimetric data of the actual sea surface height, also in relation to the reference ellipsoid. The difference between these two can obviously be considered as the actual sea surface, the (since time depending) so called dynamic topography.
We are very grateful to receive the mean sea surface model *cls01* from the French enterprise CLS (Collecte Localisation Satellites). It has been computed using a 7-year TOPEX/POSEIDON mean profile, a 5-year ERS-1/2 mean profile, a 2-year GEOSAT mean profile and the 2 168-day non repeat cycle data of the ERS-1 geodetic phase. These data were processed and homogenized using the most recent corrections to compute the CLS01 mean sea surface (CLS01 MSS) on a 1/30×1/30 degrees grid. The surface is almost global (80°S to 82°N), derived from altimetric data on oceans and from geoid undulations elsewhere (continuously connected in between, starting from an ocean depth of 10 meters).
The data set under consideration for the geoid undulations contains data on a 1/4×1/4 degree grid that spans the latitude range 85°S to 85°N. The values have been computed using the EGM96 gravitational model (see e.g. [5]) complete up to degree and order 360, and have been corrected appropriately.

Since multiscale approximations contain convolutions, this has to be evaluated by numerical integration. Obviously, two problems arise there. Primarily, numerical errors are inescapable. But by choosing the integration positions and weights properly, this can be reduced. Unfortunately, the positions are predetermined, which leads immediately to the second point. Since data positions are not arbitrary, there exists a maximal scale, from where the grid is not dense enough to justify the kernel width, i.e. a scale from where the approximation process does not converge any more. Therefore, we are confronted with the additional task to determine this optimal scale.

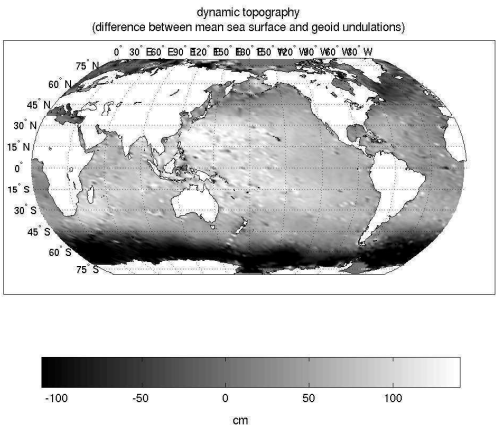

Figure 3: Original Dynamic Topography, as difference between altimetric and geoidal data sets

Combining these two initial data sets we obtain the dynamic topography as seen in Figure 3. Due to the different data density and the therefore resulting resolution difference, the dynamical topography cannot be as smooth as it should be. Thus, the multiscale approximation has the advantage of smoothing out the initial data by convolving with hat functions and at the same time giving control over the approximation rate by stopping when the hat-width becomes too small.

Its property of being a low-pass-filter is shown in comparison of Figures 4 and 5. The first one presents the multiscale approximation of Figure 3 at scale 9. Their difference (Figure 5) consists of the high-oscillating parts, which has to be smoothed out in the process. Further, Figures 4, 6 and 7 demonstrate the detail step property of multiscale approximations. Results for scales 9 (Fig. 4) and 10 (Fig. 7) present rather good results. Their difference, also computable by convolving with a wavelet of scale 9, is plotted in Figure 6. Thus, this smooth resolution process is near its end, due to only minor details remaining. The high-frequency oscillations visible in the original data (Figure 3) and filtered by the approximation (to compare see Figure 5), can be assumed to get in the way of higher scales. In fact, these are getting worse in accuracy, since the data density cannot provide enough information and the problems mentioned above occur.

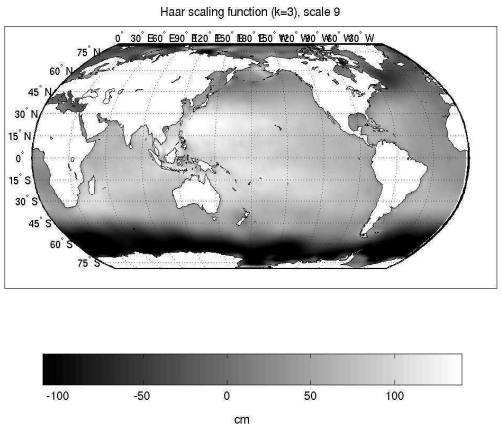

Figure 4: Multiscale Approximation at Scale 9, using the standard Haar kernel function

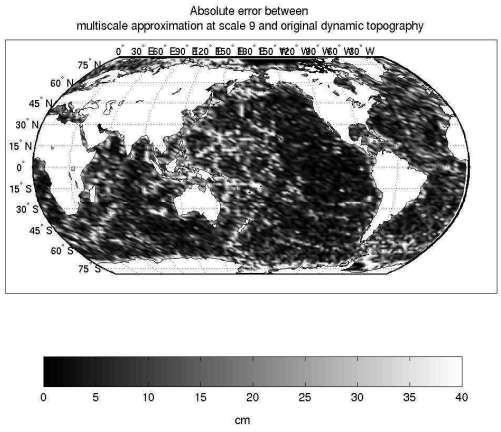

Figure 5: Error between Multiscale Approximation at Scale 9 and Dynamic Topography.

5 LARGE-SCALE ANALYSIS OF OCEANIC CURRENTS

After modeling the dynamic topography we study another application in oceanography. Making certain assumptions, modeling ocean circulation is for large-scale currents possible just from knowing the actual sea surface height, the dynamic topography. The connection between those is described by the geostrophic currents. By assuming frictionless motion (far away from coasts, ocean surfaces and ocean beds) of a homogeneous fluid,

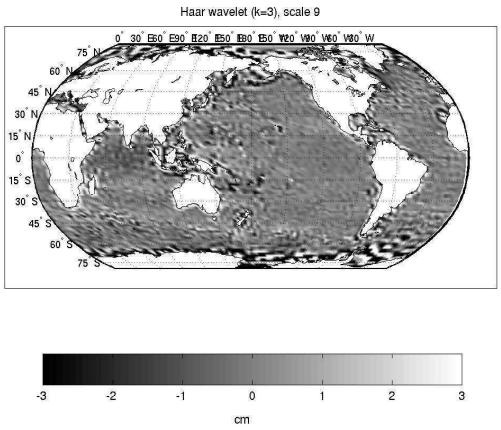

Figure 6: Wavelet Approximation at Scale 9, i.e. the difference between Scale 9 and Scale 10.

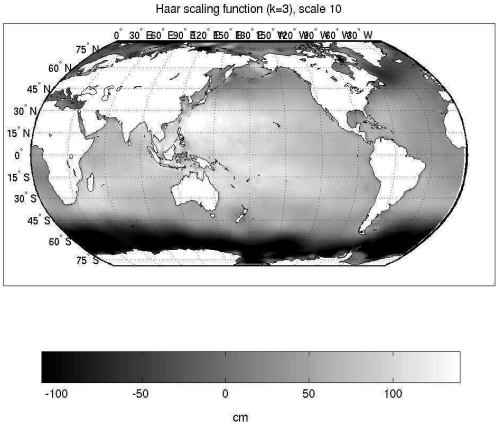

Figure 7: Multiscale Approximation at Scale 10, using the standard Haar kernel function

neglecting turbulent flows and vertical velocities, the complete Navier-Stokes equations simplify to two common conservation laws, the hydrostatic and the geostrophic balance (see e.g. [1, 6, 7]). By introducing spherical coordinates it is, therefore, possible to connect the horizontal velocity $v_{\tan}$ with the dynamic topography Ξ by a spherical differential operator, i.e.

$$v_{\tan}(\xi) = \frac{g}{f(\xi)} L_\xi^\star \Xi(\xi) \quad , \tag{4}$$

where $f(\xi) = 2|\omega|(\varepsilon^3 \cdot \xi)$ denotes the Coriolis parameter, $|\omega|$ the angular velocity of the Earth and g the acceleration of fall. Note that the surface curl gradient applied to a radial basis function is simply

$$L_\xi^\star K(\xi \cdot \eta) = (\xi \wedge \eta) K'(t)|_{t=\xi\cdot\eta} \quad . \tag{5}$$

Thus, a wavelet expansion (including numerical approximation of the integral) of a scalar field $\sum_{k=1}^N a_k K(\cdot \eta_k)$ can simply be transformed into an $L^\star$-applied version $\sum_{k=1}^N a_k (\cdot \wedge \eta_k) K'(\cdot \eta_k)$.

Using this to model the North Atlantic Ocean, we obtain the results presented in Figures 8 to 11.

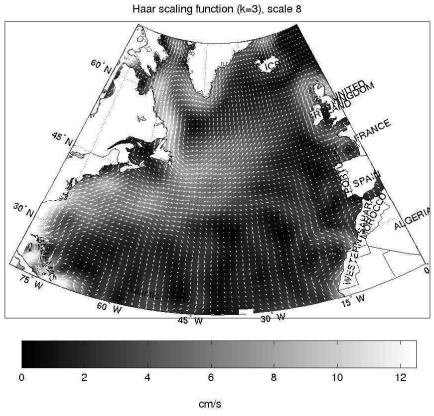

Figure 8: Multiscale Approximation at Scale 8, using the standard Haar kernel function

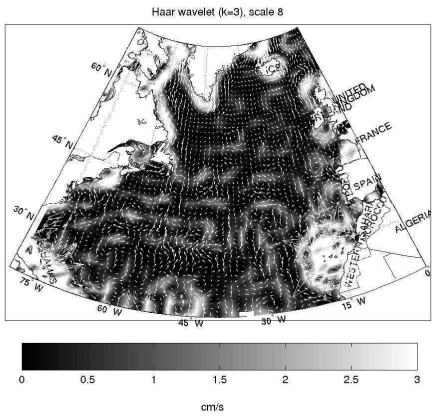

Figure 9: Wavelet Approximation at Scale 8, i.e. the difference between Scale 8 and Scale 9.

There we have multiscale approximation results of the geostrophic flow. As seen in Figure 11, the detail information summable to the approximation of scale 9 becomes worse. Although currents details are observable around the eastern coast of the United States, artifacts occur all around the tropic latitudes. These are due to resolution problems and insufficient data densities, scaled by the error sensitivity of a differential operator.

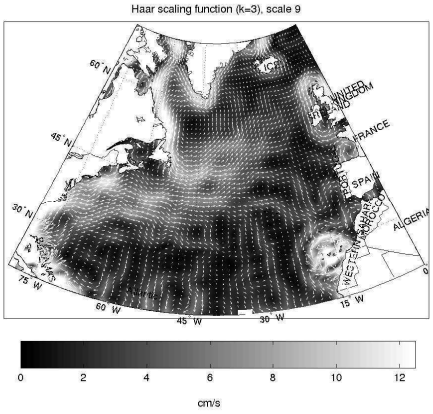

Figure 10: Multiscale Approximation at Scale 9, using the standard Haar kernel function

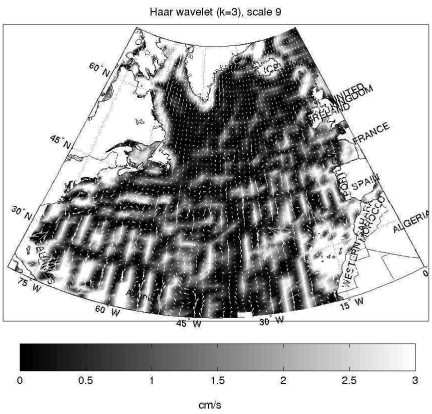

Figure 11: Wavelet Approximation at Scale 9, i.e. the detail information to obtain scale 10.

6 SUMMARY

We briefly presented a well-known system of locally supported kernels (Haar scaling functions) and its properties. Then its applicability to the modeling of the dynamic ocean topography and of the geostrophic flow has been investigated and demonstrated by numerical experiments for the first time. Where the dynamic topography has been calculated globally, we restricted our attention in case of the geostrophic flow to the North-Atlantic, where we obtained a result that clearly shows the typical form of the gulf stream. Due to the different resolution of the available sea surface and geoid models a simple plotting of the difference function yielded the expected errors, that look like a high-frequent oscillation superposing the dynamic topography. Thus, a smoothing approximation tool is required here. Whereas the spherical harmonics contain a global averaging of the data, which is certainly helpful for the representation of a global trend, the Haar scaling function is only averaging the data within a small subset of the domain due to its local support, which is advantageous with respect to efficiency of the computation and local evaluation and adaptation of the model.

References

[1] D.G. Andrews. *An Introduction to Atmospheric Physics.* Cambridge University Press, Cambridge, 2000.

[2] F. Bauer, W. Freeden, and M. Schreiner. A Tree Algorithm for Isotropic Finite Elements on the Sphere. *Numerische Mathematik (submitted)*, 2003.

[3] W. Freeden, T. Gervens, and M. Schreiner. *Constructive Approximation on the Sphere With Applications to Geomathematics.* Oxford Science Publications, Clarendon, 1998.

[4] W. Freeden and K. Hesse. On the Multiscale Solution of Satellite Problems by Use of Locally Supported Kernel Functions Corresponding to Equidistributed Data on Spherical Orbits. *Studia Scientiarum Mathematicarum Hungarica*, 39:37–74, 2002.

[5] F.G. Lemoine, S.C. Kenyon, J.K. Factor, R.G.Trimmer, N.K. Pavlis, D.S. Chinn, C.M. Cox, S.M. Klosko, S.B. Luthcke, M.H. Torrence, Y.M. Wang, R.G. Williamson, E.C. Pavlis, R.H. Rapp, and T.R. Olson. *The Development of the Joint NASA GSFC and NIMA Geopotential Model EGM96.* NASA/TP-1998-206861. NASA Goddard Space Flight Center, Greenbelt, Maryland, USA, 1998.

[6] J. Pedlosky. *Geophysical Fluid Dynamics.* Springer Verlag, New York, Heidelberg, Berlin, 1979.

[7] R.H. Stewart. *Introduction to Physical Oceanography.* electronic publication, open source, Texas University, 2003.

MULTISCALE MODELING FROM EIGEN-1S, EIGEN-2, EIGEN-GRACE01S, GGM01, UCPH2002_0.5, EGM96

Martin J. Fengler[(1)], **Willi Freeden**[(1)] **and Martin Gutting**[(1)]

[(1)] *Geomathematics Group, University of Kaiserslautern,*
P.O.Box 3049, 67653 Kaiserslautern, Germany
M. Gutting will present these results at the workshop.

Abstract

Spherical wavelets have been developed by the Geomathematics Group Kaiserslautern for several years and have been successfully applied to georelevant problems. Wavelets can be considered as consecutive band-pass filters and allow local approximations. The wavelet transform can also be applied to spherical harmonic models of the Earth's gravitational field like the most up-to-date EIGEN-1S, EIGEN-2, EIGEN-GRACE01S, GGM01, UCPH2002_0.5, and the well-known EGM96. Thereby, wavelet coefficients arise. In this paper it is the aim of the Geomathematics Group to make these data available to other interested groups. These wavelet coefficients allow not only the reconstruction of the wavelet approximations of the gravitational potential but also of the geoid, of the gravity anomalies and other important functionals of the gravitational field. Different types of wavelets are considered: bandlimited wavelets (here: Shannon and Cubic Polynomial (CuP)) as well as non-bandlimited ones (in our case: Abel-Poisson). For these types wavelet coefficients are computed and wavelet variances are given. The data format of the wavelet coefficients is also included.

Keywords: Multiscale Modeling, Wavelets, Wavelet Variances, Wavelet Coefficients, Gravitational Field Model Conversion

1 INTRODUCTION

During the last years spherical wavelets have been brought into existence (cf. e.g. [3], [4], [5] and the references therein). It is time to apply them to well-known models in order to offer easy access to the multiscale methods. Therefore, the spherical harmonics models EIGEN-1S, EIGEN-2, GGM01, UCPH2002_0.5, EGM96 and also EIGEN-GRACE01S are transformed into bilinear wavelet models (see [3], [4] or [6]) and the coefficients of these models are made available by the Geomathematics Group via the worldwide web. Moreover, the very same coefficients enable a multiscale reconstruction of the geoid, the gravity disturbance, the gravity anomalies and the vertical gravity gradients by special types of reconstructing wavelets.
Our wavelets are constructed from so-called scaling functions, i.e. kernels that depend on a scale j, of the form

$$\Phi_j(x,y) = \sum_{\substack{n=0\\n\neq 1}}^{\infty} \varphi_j(n) \frac{2n+1}{4\pi R^2} \left(\frac{R^2}{|x||y|}\right)^{n+1} P_n\left(\frac{x}{|x|}\cdot\frac{y}{|y|}\right), \quad (x,y) \in \overline{\Omega_R^{ext}} \times \overline{\Omega_R^{ext}}, \tag{1}$$

where Ω_R^{ext} denotes the outer space of the sphere Ω_R of radius R, P_n is the Legendre polynomial of degree n and $\varphi_j(n)$ is called the symbol of the scaling function. This symbol is a sequence of numbers that determines the shape of the scaling function and has special properties (for details see [2], [3] or [4]). These properties make these kernels an approximation of the Dirac distribution that converges to it for j tending to infinity. Wavelets are defined by taking the difference of two consecutive scales which is performed by the refinement equation for the symbols:

$$\psi_j(n)\tilde{\psi}_j(n) = \varphi_{j+1}^2(n) - \varphi_j^2(n), \quad n = 0,2,3,\dots . \tag{2}$$

The primal and dual wavelets Ψ_j, $\tilde{\Psi}_j$ are obtained by either taking the square root or applying the third binomial formula to equation 2. Generally, they look the following way:

$$\Psi_j(x,y) = \sum_{\substack{n=0\\n\neq 1}}^{\infty} \psi_j(n) \frac{2n+1}{4\pi R^2} \left(\frac{R^2}{|x||y|}\right)^{n+1} P_n\left(\frac{x}{|x|}\cdot\frac{y}{|y|}\right), \tag{3}$$

$$\tilde{\Psi}_j(x,y) = \sum_{\substack{n=0\\n\neq 1}}^{\infty} \tilde{\psi}_j(n) \frac{2n+1}{4\pi R^2} \left(\frac{R^2}{|x||y|}\right)^{n+1} P_n\left(\frac{x}{|x|}\cdot\frac{y}{|y|}\right). \tag{4}$$

This construction allows an approximation of level J of a potential F:

$$F_J = \Phi_J^{(2)} * F = \Phi_{J_0}^{(2)} * F + \sum_{j=J_0}^{J-1} \tilde{\Psi}_j * (\Psi_j * F) = \Phi_{J_0} * (\Phi_{J_0} * F) + \sum_{j=J_0}^{J-1} \tilde{\Psi}_j * (\Psi_j * F), \tag{5}$$

where "$*$" denotes the convolution in $\mathcal{L}^2(\Omega_R)$. These convolution integrals can be discretized for numerical evaluation by methods presented in [1] or [4]. For the wavelet coefficients that we offer to other groups we chose the equiangular grid discussed in e.g. [1].
The important examples that we used for the computation of our multiscale representations are the Shannon type, the CuP type, and the Abel-Poisson type wavelets:

1.1 Shannon Wavelets

In the case of Shannon scaling functions the symbol $\varphi_j(n)$ reads as follows

$$\varphi_j^{SH}(n) = \begin{cases} 1 & \text{for} \quad n \in [0, 2^j) \\ 0 & \text{for} \quad n \in [2^j, \infty), \end{cases} \tag{6}$$

and for the corresponding wavelets we choose the P-scale version to resolve the refinement equation (2), i.e.

$$\tilde{\psi}_j^{SH}(n) = \psi_j^{SH}(n) = \sqrt{\left(\varphi_{j+1}^{SH}(n)\right)^2 - \left(\varphi_j^{SH}(n)\right)^2}. \tag{7}$$

1.2 Cubic Polynomial (CuP) Wavelets

In the CuP case the symbol takes the following form:

$$\varphi_j^{CP}(n) = \begin{cases} (1 - 2^{-j}n)^2(1 + 2^{-j+1}n) & \text{for} \quad n \in [0, 2^j) \\ 0 & \text{for} \quad n \in [2^j, \infty) \end{cases} \tag{8}$$

and for the corresponding wavelets we apply again the P-scale version.

1.3 Abel-Poisson Wavelets

For the Abel-Poisson scaling function the symbol takes the following form $\varphi_j^{AP}(n) = e^{-2^{-j}\alpha n}$, $n \in [0, \infty)$, with some constant $\alpha > 0$. We choose $\alpha = 1$. Since $\varphi_j^{AP}(n) \neq 0$ for all $n \in \mathbb{N}$ this symbol leads to a non-bandlimited kernel. It should be noted that the Abel-Poisson scaling function has a closed form representation which allows the omission of a series evaluation and truncation, and when constructing bilinear Abel-Poisson wavelets we want to keep such a representation as an elementary function. Thus, we decide to use M-scale wavelets whose symbols are deduced from the refinement equation (2) by the third binomial formula:

$$\psi_j^{AP}(n) = \left(\varphi_{j+1}^{AP}(n) - \varphi_j^{AP}(n)\right) \qquad , \quad \tilde{\psi}_j^{AP}(n) = \left(\varphi_{j+1}^{AP}(n) + \varphi_j^{AP}(n)\right). \tag{9}$$

Since the Abel-Poisson scaling function and its corresponding wavelets are non-bandlimited we obtain just a good approximation by the numerical integration method based on an equiangular grid (we choose the parameter of polynomial exactness sufficiently large enough).

2 MULTISCALE REPRESENTATION OF THE GRAVITATIONAL POTENTIAL

The Earth's gravitational potential V in a point x of the outer space of Ω_R, i.e. the gravity potential W without the part Φ caused by centrifugal force, possesses the following representation by convolutions with scaling functions and wavelets:

$$V(x) = \int_{\Omega_R} (\Phi_{j_0} * V)(y)\Phi_{j_0}(x, y)d\omega(y) + \sum_{j=j_0}^{J_{max}-1} \int_{\Omega_R} WT_j(V; y)\tilde{\Psi}_j(x, y)d\omega(y), \tag{10}$$

where J_{max} is some suitably chosen maximal level of approximation and $WT_j(V;y) = (\Psi_j * V)(y)$ denotes the wavelet transform of V at scale j in the point y. In discrete form we get:

$$V(x) = \frac{GM}{R} \sum_{i=1}^{N_{j_0}} w_i^{j_0} v_i^{\Phi_{j_0}} \Phi_{j_0}(x, y_i^{j_0}) + \frac{GM}{R} \sum_{j=j_0}^{J_{max}-1} \sum_{i=1}^{N_j} w_i^j v_i^{\tilde{\Psi}_j} \tilde{\Psi}_j(x, y_i^j) \,. \tag{11}$$

The weights of the integration are named $w_i^{j_0}$, w_i^j and the corresponding knots are $y_i^{j_0}$, y_i^j. The scaling function coefficients $v_i^{\Phi_{j_0}}$ and the wavelet coefficients $v_i^{\tilde{\Psi}_j}$ result from the convolutions (12):

$$\frac{GM}{R} v_i^{\Phi_{j_0}} = (\Phi_{j_0} * V)(y_i^{j_0}) \,, \qquad \frac{GM}{R} v_i^{\tilde{\Psi}_j} = WT_j(V; y_i^j) = (\Psi_j * V)(y_i^j). \tag{12}$$

Fig. 1 and 2 show examplarily a part of the multiscale resolution of (10) where the details (Fig. 2) are added to the approximation of scale 7 (Fig. 1). By subtracting the non-centrifugal part of the ellipsoidal normal

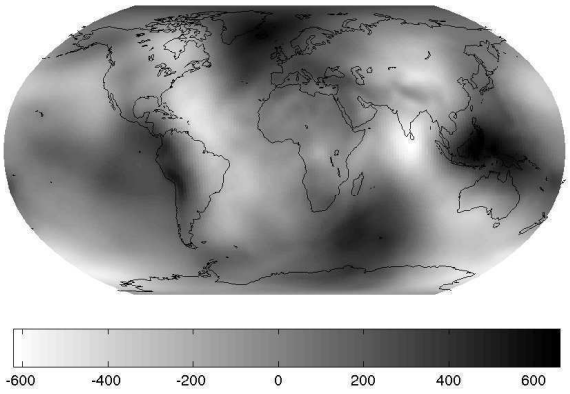

Figure 1: Approximation at Scale 7 of V from EIGEN2 using the CuP scaling function, $[m^2/s^2]$.

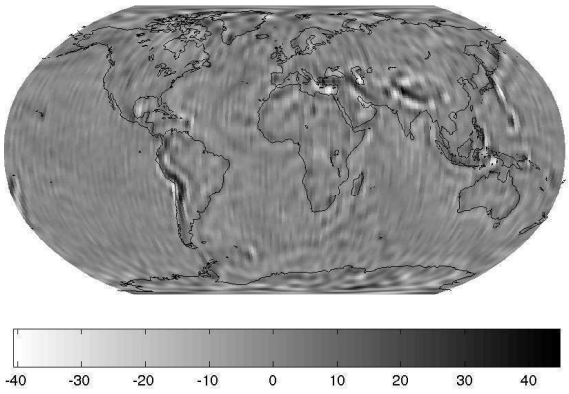

Figure 2: Wavelet detail at scale 7 of V from EIGEN2 using the CuP wavelet, $[m^2/s^2]$.

potential $V_{ell} = U - \Phi$ from V the disturbing potential $T = V - V_{ell}$ can be obtained (see [7], [8] or [9]) and this subtraction can be performed for the coefficients $v_i^{\Phi_{j_0}}$, $v_i^{\tilde{\Psi}_j}$ in order to obtain a multiscale representation of the disturbing potential similar to (11), but with coeffients $t_i^{\Phi_{j_0}}$ and $t_i^{\tilde{\Psi}_j}$ that are related to $v_i^{\Phi_{j_0}}$, $v_i^{\tilde{\Psi}_j}$ by the equations (13):

$$\frac{GM}{R} t_i^{\Phi_{j_0}} = \frac{GM}{R} v_i^{\Phi_{j_0}} - (\Phi_{j_0} * V_{ell})(y_i^{j_0}) \,, \qquad \frac{GM}{R} t_i^{\tilde{\Psi}_j} = \frac{GM}{R} v_i^{\tilde{\Psi}_j} - (\Psi_j * V_{ell})(y_i^j) \tag{13}$$

A more detailed derivation can be found in [2].

3 FUNCTIONALS OF THE DISTURBING POTENTIAL

By virtue of the Bruns formula $N = T/\gamma$ (cf. [7], [8] or [9]) a multiscale representation of the *geoid undulations* can be computed from the multiscale decomposition of the disturbing potential, i.e. from the coefficients $t_i^{\Phi_{j_0}}$ and $t_i^{\tilde{\Psi}_j}$. Thereby, the normal gravity γ is taken spherically as $\gamma = \frac{GM}{R^2}$. Thus, the geoid heights N are described by

$$N(x) = R \sum_{i=1}^{N_{j_0}} w_i^{j_0} t_i^{\Phi_{j_0}} \Phi_{j_0}(x, y_i^{j_0}) + R \sum_{j=j_0}^{J_{max}-1} \sum_{i=1}^{N_j} w_i^j t_i^{\tilde{\Psi}_j} \tilde{\Psi}_j(x, y_i^j) \,. \tag{14}$$

In Fig. 3 and 4 parts of a multiresolution of N are presented (see [2] for a full multiresolution).

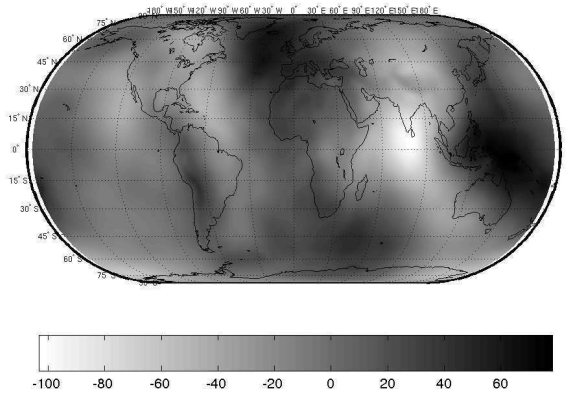

Figure 3: Multiscale geoid heights N at Scale 7 from EGM96 using the CuP scaling function, $[m]$.

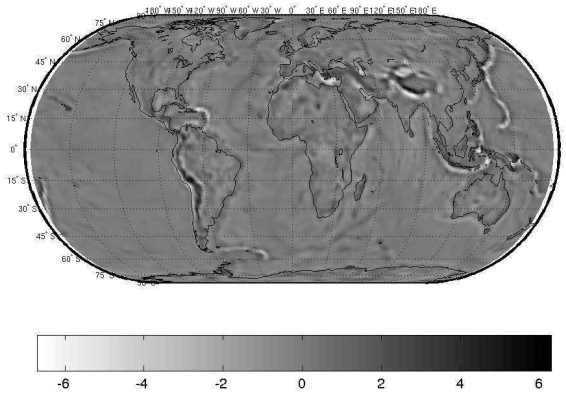

Figure 4: Wavelet detail at scale 7 of geoid heights N from EGM96 using the CuP wavelet, $[m]$.

By definition the *gravity disturbances* correspond to the negative first radial derivative of T which leads to the multiscale representation (15):

$$\begin{aligned}\delta g(x) &= -\frac{GM}{R}\left(\sum_{i=1}^{N_{j_0}} w_i^{j_0} t_i^{\Phi_{j_0}} \frac{\partial}{\partial r_x}\Phi_{j_0}(x,y_i^{j_0}) + \sum_{j=j_0}^{J_{max}-1}\sum_{i=1}^{N_j} w_i^j t_i^{\tilde{\Psi}_j} \frac{\partial}{\partial r_x}\tilde{\Psi}_j(x,y_i^j)\right)\\ &= \frac{GM}{R|x|}\sum_{i=1}^{N_{j_0}} w_i^{j_0} t_i^{\Phi_{j_0}} \Phi_{j_0}^{\delta g}(x,y_i^{j_0}) + \frac{GM}{R|x|}\sum_{j=j_0}^{J_{max}-1}\sum_{i=1}^{N_j} w_i^j t_i^{\tilde{\Psi}_j}\tilde{\Psi}_j^{\delta g}(x,y_i^j) \end{aligned} \tag{15}$$

with

$$\Phi_{j_0}^{\delta g}(x,y_i^{j_0}) = -|x|\frac{\partial}{\partial r_x}\Phi_{j_0}(x,y_i^{j_0}) = \sum_{\substack{n=0\\ n\neq 1}}^{\infty}\varphi_j^{\delta g}(n)\frac{2n+1}{4\pi R^2}\left(\frac{R^2}{|x||y_i^{j_0}|}\right)^{n+1} P_n\left(\frac{x}{|x|}\cdot\frac{y_i^{j_0}}{|y_i^{j_0}|}\right) \tag{16}$$

where $\varphi_j^{\delta g}(n) = (n+1)\varphi_j(n)$ and the corresponding reconstructing wavelets $\tilde{\Psi}_j^{\delta g}$ are constructed by applying the symbol $\tilde{\psi}_j^{\delta g}(n) = (n+1)\tilde{\psi}_j(n)$.
Analogously, the multiscale descriptions of the *gravity anomalies* $\Delta g = \delta g - \frac{2}{|x|}T$ and the *vertical gravity gradients* $g_r = \frac{\partial^2 T}{\partial r^2}$ assume the following shape:

$$\Delta g(x) = \frac{GM}{R|x|}\sum_{i=1}^{N_{j_0}} w_i^{j_0} t_i^{\Phi_{j_0}} \Phi_{j_0}^{\Delta g}(x,y_i^{j_0}) + \frac{GM}{R|x|}\sum_{j=j_0}^{J_{max}-1}\sum_{i=1}^{N_j} w_i^j t_i^{\tilde{\Psi}_j}\tilde{\Psi}_j^{\Delta g}(x,y_i^j)\,, \tag{17}$$

$$g_r(x) = \frac{GM}{R|x|^2}\sum_{i=1}^{N_{j_0}} w_i^{j_0} t_i^{\Phi_{j_0}} \Phi_{j_0}^{g_r}(x,y_i^{j_0}) + \frac{GM}{R|x|^2}\sum_{j=j_0}^{J_{max}-1}\sum_{i=1}^{N_j} w_i^j t_i^{\tilde{\Psi}_j}\tilde{\Psi}_j^{g_r}(x,y_i^j)\,, \tag{18}$$

where

$$\Phi_{j_0}^{\Delta g}(x,y_i^{j_0}) = \sum_{\substack{n=0\\ n\neq 1}}^{\infty}\varphi_j^{\Delta g}(n)\frac{2n+1}{4\pi R^2}\left(\frac{R^2}{|x||y_i^{j_0}|}\right)^{n+1} P_n\left(\frac{x}{|x|}\cdot\frac{y_i^{j_0}}{|y_i^{j_0}|}\right)\,, \tag{19}$$

$$\Phi_{j_0}^{g_r}(x,y_i^{j_0}) = |x|^2\frac{\partial^2}{\partial r_x^2}\Phi_{j_0}(x,y_i^{j_0}) = \sum_{\substack{n=0\\ n\neq 1}}^{\infty}\varphi_j^{g_r}(n)\frac{2n+1}{4\pi R^2}\left(\frac{R^2}{|x||y_i^{j_0}|}\right)^{n+1} P_n\left(\frac{x}{|x|}\cdot\frac{y_i^{j_0}}{|y_i^{j_0}|}\right) \tag{20}$$

with the symbols

$$\varphi_j^{\Delta g}(n) = \varphi_j^{\delta g}(n) - 2\varphi_j(n) = (n-1)\varphi_j(n) \qquad , \quad \varphi_j^{g_r}(n) = (n+1)(n+2)\varphi_j(n)\,, \tag{21}$$

and corresponding symbols $\tilde{\psi}_j^{\Delta g}(n)$ and $\tilde{\psi}_j^{g_r}(n)$ for the respective wavelets. As an example we show in Fig. 5 and 6 for the gravity anomalies Δg again scale and detail 7 with CuP scaling functions or wavelets, respectively.

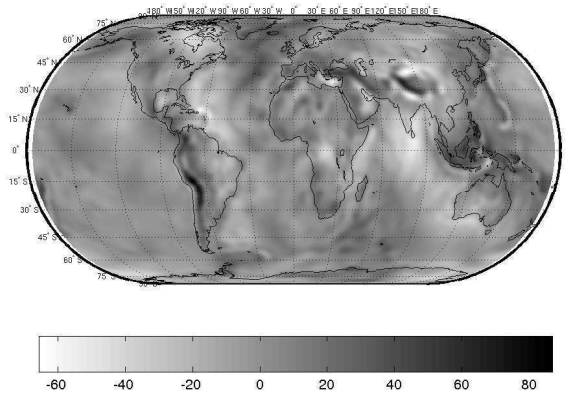

Figure 5: Δg at Scale 7 from EGM96 using CuP, $[mgal]$.

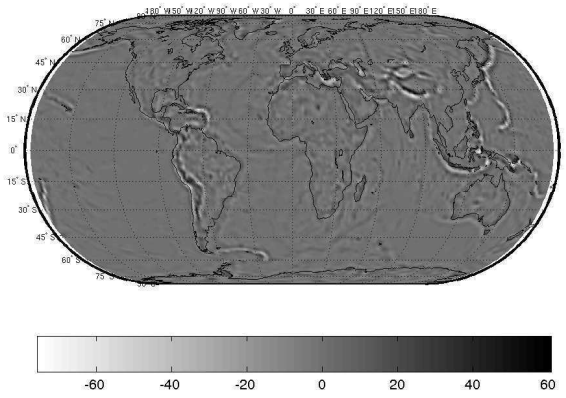

Figure 6: Wavelet detail at scale 7 of Δg from EGM96 using CuP, $[mgal]$.

4 WAVELET VARIANCES

The distribution of space-dependent signal energy of the disturbing potential is described by the *scale and space variances* of T at scale j and point x (see [2], [5]):

$$\mathrm{Var}_{j\,;\,x}(T) = \sigma^2_{j\,;\,x}(T) = \int_{\Omega_R}\int_{\Omega_R} T(y)T(z)\Psi_j(y,x)\Psi_j(z,x)d\omega(y)d\omega(z)\,. \tag{22}$$

Using the wavelet coefficients $t_i^{\tilde{\Psi}_j}$ one can compute this quantity with the help of a Shannon kernel $SH(\cdot\,,\,\cdot)$ as

$$\sigma_{j\,;\,x}(T) = \frac{GM}{R}\sigma_{j\,;\,x} \qquad , \quad \sigma^2_{j\,;\,x} = \left(\sum_{i=1}^{N_j} w_i^j t_i^{\tilde{\Psi}_j} SH(y_i^j, x)\right)^2 . \tag{23}$$

The wavelet variances of the geoidal heights N are then given by $\sigma_{j\,;\,x}(N) = R\sigma_{j\,;\,x}$; and for the gravity disturbances, the gravity anomalies, and the vertical gravity gradients the variances can be obtained by a convolution with special Shannon kernels similar to (16), (19) and (20):

$$\sigma^2_{j\,;\,x}(\delta g) = \left(\frac{GM}{R|x|}\sum_{i=1}^{N_j} w_i^j t_i^{\tilde{\Psi}_j} SH^{\delta g}(y_i^j, x)\right)^2 , \tag{24}$$

$$\sigma^2_{j\,;\,x}(\Delta g) = \left(\frac{GM}{R|x|}\sum_{i=1}^{N_j} w_i^j t_i^{\tilde{\Psi}_j} SH^{\Delta g}(y_i^j, x)\right)^2 , \tag{25}$$

$$\sigma^2_{j\,;\,x}(g_r) = \left(\frac{GM}{R|x|^2}\sum_{i=1}^{N_j} w_i^j t_i^{\tilde{\Psi}_j} SH^{g_r}(y_i^j, x)\right)^2 . \tag{26}$$

Fig. 7 to 10 demonstrate the development of the energy distribution of the disturbing potential for $j = 4$ to 7.

5 WAVELET COEFFICIENTS

We supply to the end-user the scaling function or wavelet coefficients, $v_i^{\Phi_{j_0}}$ or $v_i^{\tilde{\Psi}_j}$ corresponding to the locations of the equiangular grid on Ω_R as well as the integration weights $w_i^{j_0}$, w_i^j. The wavelet coefficients are ordered as

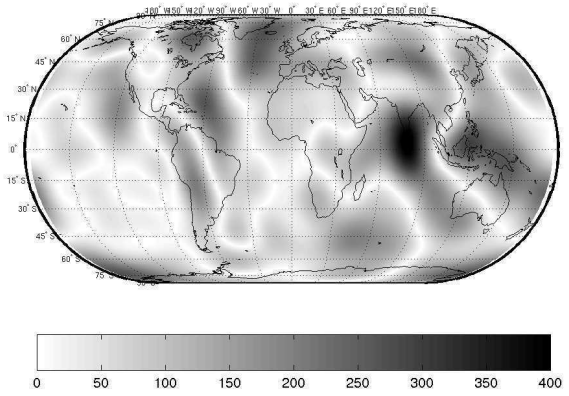

Figure 7: $\sigma_{4;\,x}(T)$ (rescaled to maximal 400), $[m^2/s^2]$.

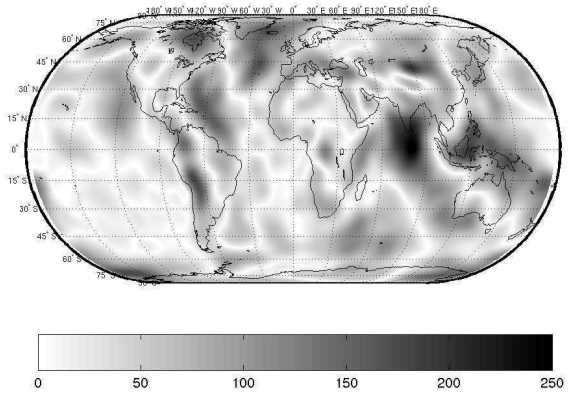

Figure 8: $\sigma_{5;\,x}(T)$ (rescaled to maximal 250), $[m^2/s^2]$.

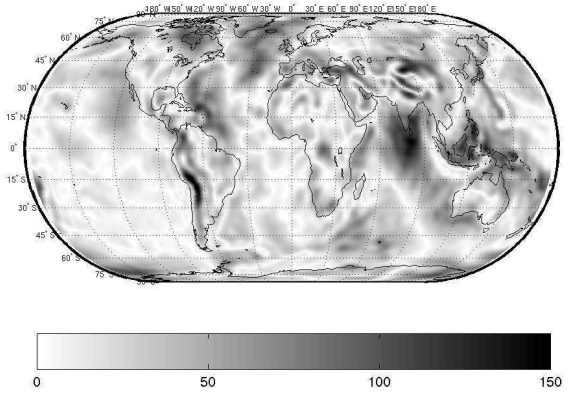

Figure 9: $\sigma_{6;\,x}(T)$ (rescaled to maximal 150), $[m^2/s^2]$.

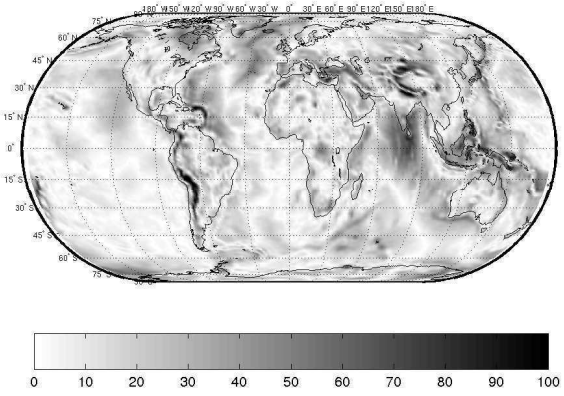

Figure 10: $\sigma_{7;\,x}(T)$ (rescaled to max. 100), $[m^2/s^2]$.

a square matrix, in addition the weights form a first column. Comments are located in the first 20 lines of the file and are indicated by a % sign. The coefficients, a detailed model description and further figures can be found and downloaded at the following web page: `http://www.mathematik.uni-kl.de/~wwwgeo/waveletmodels.html`

References

[1] Driscoll J. R., Healy D. M., *Computing Fourier Transforms and Convolutions on the 2-Sphere*, Adv. Appl. Math., Vol. 15, 202–250, 1994.

[2] Fengler M. J., Freeden W., Gutting M., *Darstellung des Gravitationsfelds und seiner Funktionale mit Multiskalentechniken*, Zeitschrift für Vermessungswesen (ZfV), 2004. (submitted)

[3] Freeden W., *Multiscale Modelling of Spaceborne Geodata*, BG Teubner, Stuttgart, Leipzig, 1999.

[4] Freeden W., Gervens T., Schreiner M., *Constructive Approximation on the Sphere (With Applications to Geomathematics)*, Oxford Science Publications, Clarendon, Oxford, 1998.

[5] Freeden W., Maier T., *On Multiscale Denoising of Spherical Functions: Basic Theory and Numerical Aspects*, Electron. Trans. Numer. Anal. (ETNA), Vol. 14, 40–62, 2002.

[6] Freeden W., Michel V., *Multiscale Potential Theory (with Application to Earth's Sciences)*, Birkhäuser, 2004. (in print)

[7] Groten E., *Geodesy and the Earth's Gravity Field I, II*, Dümmler, 1979.

[8] Heiskanen W. A., Moritz H., *Physical Geodesy*, W. H. Freeman and Company, 1967.

[9] Torge W., *Geodäsie*, Sammlung Göschen, de Gruyter, 1975.

Folgende Berichte sind erschienen:

2003

Nr. 1 S. Pereverzev, E. Schock.
On the adaptive selection of the parameter in regularization of ill-posed problems

Nr. 2 W. Freeden, M. Schreiner.
Multiresolution Analysis by Spherical Up Functions

Nr. 3 F. Bauer, W. Freeden, M. Schreiner.
A Tree Algorithm for Isotropic Finite Elements on the Sphere

Nr. 4 W. Freeden, V. Michel (eds.)
Multiscale Modeling of CHAMP-Data

Nr. 5 C. Mayer
Wavelet Modelling of the Spherical Inverse Source Problem with Application to Geomagnetism

2004

Nr. 6 M.J. Fengler, W. Freeden, M. Gutting
Darstellung des Gravitationsfelds und seiner Funktionale mit Multiskalentechniken

Nr. 7 T. Maier
Wavelet-Mie-Representations for Soleniodal Vector Fields with Applications to Ionospheric Geomagnetic Data

Nr. 8 V. Michel
Regularized Multiresolution Recovery Of the Mass Density Distribution From Satellite Data of the Earth's Gravitational Field

Nr. 9 W. Freeden, V. Michel
Wavelet Deformation Analysis for Spherical Bodies

Nr. 10 M. Gutting, D. Michel (eds.)
Contributions of the Geomathematics Group, TU Kaiserlautern, to the 2nd International GOCE User Workshop at ESA-ESRIN Frascati, Italy

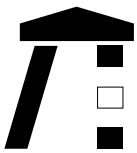

TECHNISCHE UNIVERSITÄT
KAISERSLAUTERN

Informationen:

Prof. Dr. W. Freeden
Prof. Dr. E. Schock
Fachbereich Mathematik
Technische Universität Kaiserslautern
Postfach 3049
D-67653 Kaiserslautern
E-Mail: freeden@mathematik.uni-kl.de
schock@mathematik.uni-kl.de